Further accuracy verification of the 2D adaptive mesh refinement method by the benchmarks of lid-driven cavity flows

Rajnesh Lal[1], *†Zhenquan Li[2] and Miao Li[3]

[1]School of Mathematical and Computing Sciences, Fiji National University, Lautoka, Fiji
[2]School of Computing and Mathematics, Charles Sturt University, Thurgoona, NSW 2640, Australia
[3]CSU Engineering, Charles Sturt University, Bathurst, NSW 2795, Australia
*Presenting author: jali@csu.edu.au
†Corresponding author: jali@csu.edu.au

Abstract

The lid-driven cavity flow problem is a well-known test case in fluid dynamics for validating computational fluid dynamics (CFD) algorithms. Despite its geometrical simplicity, the lid-driven cavity flow problem exhibits a complex flow regime, mainly due to the vortices formed in the centre and at the corners of the square domain. Consequently, this paper verifies the accuracy of a 2D adaptive mesh refinement (AMR) method in estimating the locations of the centre of vortices for a steady incompressible flow in a 2D lid-driven square cavity. We consider an initial coarse uniform grid mesh with a resolution of 20×20 and 50×50 for Reynolds number $Re = 1000$ and 2500, respectively and perform ten refinements. Our study reports the location of the centre of vortices obtained for $Re = 1000$ and 2500. The accuracy of the result is shown by comparing the coordinates of centres of vortices located by the AMR method with the corresponding benchmark results from four different literature.

Keywords: Adaptive mesh refinement, Refined mesh, Lid driven cavity, Centre of vorticies.

Introduction

Computational Fluid Dynamics (CFD) has evolved into a powerful tool for simulating fluid flow, heat transfer, and other related phenomena in diverse engineering applications. The discretization of the computing domain through a mesh is crucial to accurate and robust CFD simulations. Mesh refinement, a crucial aspect of this discretization process, involves adjusting the grid resolution to capture fine details and complex flow features.

Mesh generation and adaptivity remain major obstacles in the CFD workflow. Ensuring consistent and dependable convergence of flow solvers and residual values poses challenges in various industrial scenarios [1]. While numerous CFD software packages can achieve convergence in simpler scenarios, they often struggle with flows involving difficult flow physics and/or complex geometries, such as those encountered in high-lift aircraft configurations. Many existing solver techniques lack the robustness required to guarantee reliable convergence in such cases. Adaptive mesh refinement (AMR) is a computational strategy allowing users to optimise their simulations by dynamically modifying the resolution of the computational mesh in accordance with evolving flow characteristics and phenomena, thereby decreasing computational cost. AMR techniques often adjust the computational mesh during the time-stepping process, refining it selectively in areas of interest or where refinement is deemed necessary [2, 3]. Although AMR strategies offer the potential for increased accuracy at a lower computational cost, their adoption has been limited by concerns regarding robustness, error estimation, management of complex geometries, and software complexity issues [1].

In tackling the complexities of accurately simulating fluid flow problems while maintaining computational efficiency, the AMR technique has undergone significant evolution, driven by contributions from various researchers in the CFD domain. The origin of adaptive mesh refinement for CFD can be traced back to the 1980s and 1990s, encompassing seminal works by researchers such as Berger and Oliger [4], Bell *et al*. [5], Friedel *et al*. [6], and Berger and Leveque [7]. Since then, the development of AMR has continued to evolve with advancements in numerical methods, computer hardware and software tools, and applied to a variety of fluid dynamics and computational science problems.

Li [8] introduced a 2D AMR technique derived from the qualitative theory of differential equations. This AMR method refines a computational mesh using numerically computed velocity fields. The efficacy and accuracy of this AMR method have been verified through the accurate locations of singular points, asymptotic lines, and closed streamlines [9], as well as through comparisons with established CFD benchmark experiments up to two refinements, including lid-driven cavity flow [10], 2D unsteady flow past a square cylinder [11], backwards-facing step flow [12], and 2D flow over a wall-mounted plate [13]. Furthermore, the AMR method has demonstrated its capability to capture localized flow features, such as identifying accurate locations of the centre of vortices within refined cells [10, 13]. The accuracy of the AMR method depends solely on the accuracy of the numerical methods used. The AMR method is a low-cost and robust method applicable to all incompressible fluid flows [10, 2].

The lid-driven cavity flow problem is a well-known test case in fluid dynamics for validating CFD algorithms. Even though the lid-driven cavity flow problem appears geometrically simple, it exhibits a complex flow regime primarily attributable to the formation of vortices at the centre and corners of the square domain. The combination of its simple geometry, the presence of various corner singularities, and the difficulty in approximating the exact solution made the lid-driven cavity one of the most common benchmarks in CFD. Several benchmark results are available in the literature, including the works of Ghia *et al*. [14], Botella and Peyret [15], Erturk *et al*. [16], and Shapeev and Lin [17], among others. Ghia *et al*. [14] used the vorticity-stream function formulation of the 2D incompressible Navier-Stokes (N-S) equations to study the effectiveness of the coupled strongly implicit multigrid method. The solution for flows with several Reynolds numbers (Re) is computed. For $Re = 1000$, the fine-mesh flow solution using the uniform grid mesh of resolution 129×129 is reported. Botella and Peyret [15] reported the solutions for the lid-driven cavity flow for $Re = 1000$, computed by a Chebyshev collocation method with a grid mesh of $N = 160$ (polynomial degree). Erturk *et al*. [16] have used the N-S equations in stream function and vorticity formulation, which are solved numerically using a fine uniform grid mesh of 601×601. The solution for flows computed with several high $Re \leq 21000$ are reported. Shapeev and Lin [17] have used the stream function formulation of the N-S equations for the solution of the lid-driven cavity flow with several Re. In [17], the problem is approached using a high-order finite element technique featuring exponential mesh refinement in proximity to the corners, coupled with analytical asymptotics of the flow near the corners. For $Re = 1000$ and 2500, the results using 49156 triangular elements are presented in [17].

The earlier works, e.g. [2, 10], examined the accuracy of the 2D AMR method with two refinements and used the finite volume methods to solve the N-S equations numerically. As the 2D AMR technique can be iteratively applied, greater accuracy in locating vortex centres can be achieved if numerical velocity fields are sufficiently accurate and additional refinements are implemented. Hence, the present study further verifies the accuracy of a 2D AMR method in estimating the locations of the centre of vortices for a steady incompressible flow in a 2D

lid-driven square cavity using additional mesh refinements. A finite element method is used to solve the N-S equations numerically. We consider an initial coarse uniform grid mesh with a resolution of 20×20 and 50×50 for Reynolds number $Re = 1000$ and 2500, respectively and perform ten refinements. The accuracy of the results obtained for $Re = 1000$ and 2500 are demonstrated by comparing the coordinates of centres of vortices located by the AMR method with the corresponding benchmark results from those presented in [14, 15, 16, 17].

Method

This section describes the governing equations, the computational domain and the mesh structure, the flow solver, and briefly on the 2D AMR method.

The governing equations and computational domain

The present study consider the finite element discretizations of the 2D steady, incompressible Navier-Stokes equations, which are governed by the continuity equation and the momentum equations in two directions defined by:

$$\begin{aligned} \nabla \cdot \mathbf{V} &= 0 \\ -\nu \nabla^2 \mathbf{V} + \mathbf{V} \cdot \nabla \mathbf{V} + \frac{1}{\rho} \nabla P &= 0, \end{aligned}$$

where $\mathbf{V} = (u, v)$ denotes the velocity field in 2D with u as the velocity component at the x-direction and v as the velocity component at the y-direction, ν is the kinematic viscosity, ρ is the fluid density, and P represents the scalar pressure.

The lid-driven cavity consists of a square cavity with the dimensions of L. At the top boundary, a tangential unit velocity ($u = 1, v = 0$) is applied to drive the fluid flow in the cavity. The remaining three rigid walls are imposed with no-slip boundary conditions ($u = v = 0$). The origin of the cartesian coordinate is located at the left lower corner of the cavity. The geometry of the computational domain is shown in Figure 1. The Reynolds number is defined as $Re = UL/\nu$, where U is the velocity of the lid, L is the length of the cavity, and ν is the kinematic viscosity of the fluid.

Computational mesh and the flow solver

For the case with $Re = 1000$, the initial mesh (Mesh_0) is a uniform grid mesh with resolution of 20×20, i.e. Mesh_0 has 441 computational nodes. This corresponds to 1323 degrees of freedom (DOF). The DOF is given by the number of nodes multiplied by the number of dependent variables. For $Re = 2500$, Mesh_0 is a uniform grid mesh with a resolution of 50×50 corresponding to 2601 computational nodes and 7803 DOF. The `Finite Element Analysis simulation Toolbox` (`FEATool`, version 1.16.3, https://www.featool.com/) in `MATLAB` (R2023a) was used to numerically solve the steady 2D Navier-Stokes equations. We assumed that the convergence is achieved when the numerical solutions (velocity fields) are computed with residuals smaller than 10^{-12}.

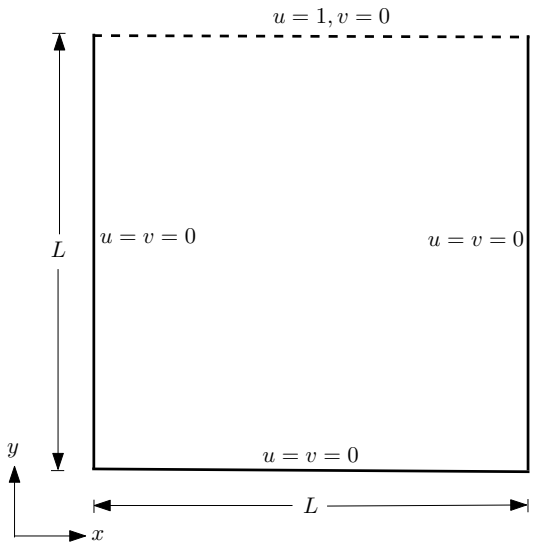

Figure 1: Cavity flow geometry and boundary conditions.

The 2D adaptive mesh refinement method

In the present study, we apply the same AMR method from [13]. We summarise the 2D AMR method and further refer the reader to Section 3 of [13] for a detailed description of the method.

Let $\mathbf{V}_l = \mathbf{AX}+\mathrm{b}'$ be defined as a vector field on a triangle obtained through linear interpolation of vectors at the three vertices of the triangle in the domain of the velocity field, where

$$\mathbf{A} = \begin{pmatrix} a_{11} & a_{12} \\ a_{21} & a_{22} \end{pmatrix}, \ \mathbf{b}' = \begin{pmatrix} b'_1 \\ b'_2 \end{pmatrix}, \text{ and } \mathbf{X} = \begin{pmatrix} x_1 \\ x_2 \end{pmatrix}$$

is a matrix of constants, a vector of constants, and a vector of spatial variables, respectively.

For the interpolated vector field $\mathbf{V}_l$ to satisfy the continuity equation for incompressible or steady-state flow, the equation $\nabla \cdot \mathbf{V}_l = \text{trace}(\mathbf{A}) = 0$ must be satisfied. However, the interpolated numerical velocity vector field generally does not satisfy the continuity equation. Hence, it is assumed that $f\mathbf{V}_l$ satisfies the continuity equation, where f is an unknown scalar function of the spatial variables x_1 and x_2. A differential equation is obtained when $f\mathbf{V}_l$ is substituted into the vector field $\mathbf{V}$ of the continuity equation $\nabla \cdot \mathbf{V} = 0$, resulting in $\nabla \cdot f\mathbf{V}_l = 0$. Solving the resulting differential equation for the four different Jacobian forms of the constant matrix $\mathbf{A}$ results in four distinct expressions of the function f. Table 1 shows the summary of the Jacobian forms of the constant matrix $\mathbf{A}$ with their corresponding distinct expressions of the function f for the four distinct cases in which the linear interpolations of the vector fields over triangular domains do not satisfy the law of mass conservation.

In Table 1, $(y_1, y_2)^T = \mathbf{V^{-1}X}$ and $(b_1, b_2)^T = \mathbf{V^{-1}b}$ where $\mathbf{V}$ satisfies $\mathbf{AV} = \mathbf{VJ}$, and $\mathbf{J}$ is one of the Jacobian matrices in the table. For $f \notin \{0, \infty\}$, the vectors $\mathbf{V}_l$ and $f\mathbf{V}_l$ produce same streamlines (for more details we refer the readers to Section 2.2 of [9]). Consequently, mass conservation (MC) conditions are that the computed functions f in Table 1 are not equal to zero or infinity at any point on the triangular domains.

A cell-by-cell AMR approach is performed on the quadrilateral grid meshes. A quadrilateral cell on which one of the conditions MC is not satisfied is subdivided. A cell is refined by connecting the mid-points of opposite sides into four equally smaller quadrilateral cells. Applying the AMR

Table 1: Jacobian forms of the constant matrix A and the corresponding distinct expressions of the function f ($C \neq 0$) for all possible cases of a non-mass conservative linear field. The value of C is set to 1 when the conditions (MC) are implemented in `MATLAB`.

Case	Jacobian	f
1	$\begin{pmatrix} r_1 & 0 \\ 0 & r_2 \end{pmatrix}$ $(0 \neq r_1 \neq r_2 \neq 0)$	$\frac{C}{\left(y_1+\frac{b_1}{r_1}\right)\left(y_2+\frac{b_2}{r_2}\right)}$
2	$\begin{pmatrix} r_1 & 0 \\ 0 & 0 \end{pmatrix}$ $(r_1 \neq 0)$	$\frac{C}{y_1+\frac{b_1}{r_1}}$
3	$\begin{pmatrix} r_1 & 0 \\ 0 & r_1 \end{pmatrix}$ $(r_1 \neq 0)$	$\frac{C}{\left(y_1+\frac{b_1}{r_1}\right)^2}$
4	$\begin{pmatrix} \mu & \lambda \\ -\lambda & \mu \end{pmatrix}$ $(\mu \neq 0, \lambda \neq 0)$	$\frac{C}{\left(y_1+\frac{\mu b_1-\lambda b_2}{\mu^2+\lambda^2}\right)^2+\left(y_2+\frac{\lambda b_1+\mu b_2}{\mu^2+\lambda^2}\right)^2}$

method to the initial mesh, Mesh_0, produces the first refined mesh, Mesh_1, and by repeating the procedure nine more times, we obtain the tenth refined mesh, Mesh_{10}. The coordinates of the centre of the isolated refined cells in the area of interest are then taken as an estimate of the centre of vortices.

Numerical results and accuracy verification

This section shows the tenth refined meshes, Mesh_{10}, and the vortices' locations generated in a driven cavity flow for $Re = 1000$ and 2500. The abbreviations BR, BL and TL refer to the bottom right, bottom left and top left, respectively. The number following the abbreviations refers to the vortices that appear in the flow, numbered in order of decreasing size. The abbreviation PV refers to the primary vortex. We then compare estimated centres of PV, BR1, BL1, BR2, BL2 and TL1 with the benchmark results.

The refined meshes, Mesh$_{10}$

Figure 2 shows the tenth refined mesh, Mesh_{10}, for the flow with $Re = 1000$. Figure 3(a)-(e) shows the isolated refined cells containing the centres of vortices in the zoomed-in sections of PV, BR and BL. In Figure 3, red circles are drawn for illustration, and they contain the location of the centres of PV, BR1, BL1, BR2 and BL2 for $Re = 1000$. To validate the local accuracy of the numerically computed velocity fields for the case with $Re = 1000$, in Figures 4 and 5, we present the u-velocity profile along a vertical line and the v-velocity profile along a horizontal line passing through the geometric centre of the cavity, respectively. These profiles agree well with Erturk *et al*. [16], as shown by the symbols in Figures 4 and 5.

For the flow with $Re = 2500$, a similar mesh refinement pattern as for the flow with $Re = 1000$ was observed. Figure 6 shows Mesh_{10} for the flow with $Re = 2500$. The refined mesh in Figure 6 identifies the location of an additional secondary vortex, TL1, which appears near the top left corner. Figures 7 and 8 compare the u and v-velocity profiles, respectively, with the benchmark results of Erturk *et al*. [16]. We observe a good agreement between the numerically computed velocity fields and those reported in [16].

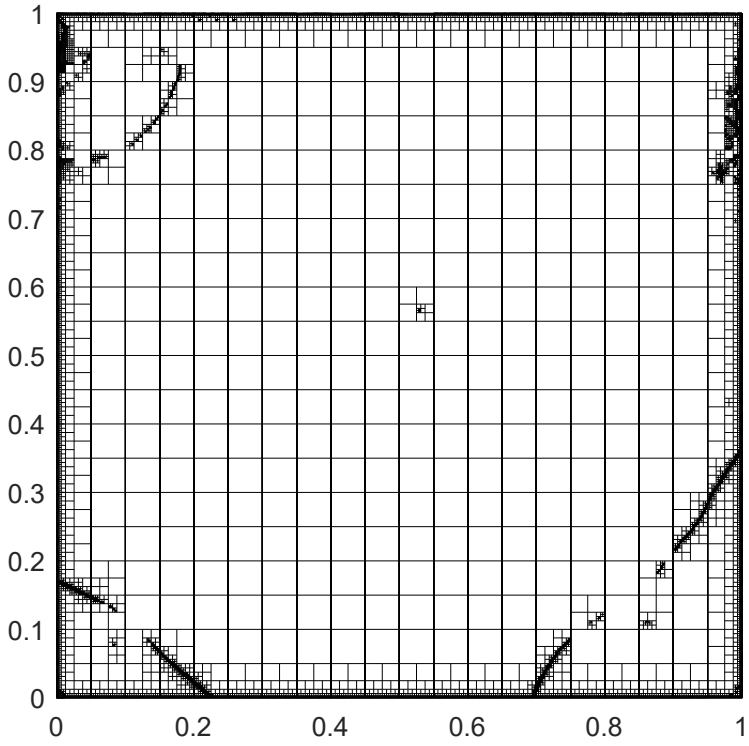

Figure 2: The tenth refined mesh, Mesh$_{10}$, for the flow with $Re = 1000$.

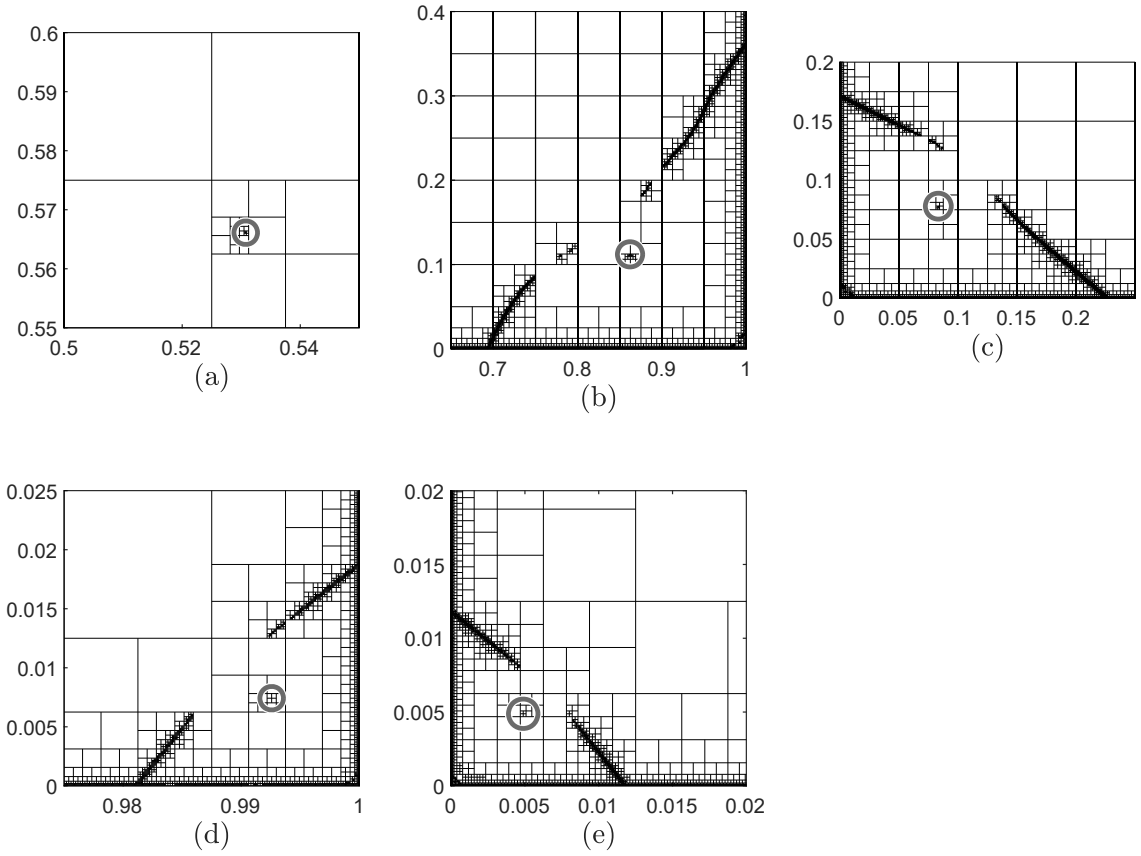

Figure 3: Zoomed-in sections of PV, BR and BL for $Re = 1000$. Red circles contain the location of the centres of (a) PV, (b) BR1, (c) BL1, (d) BR2 and (e) BL2.

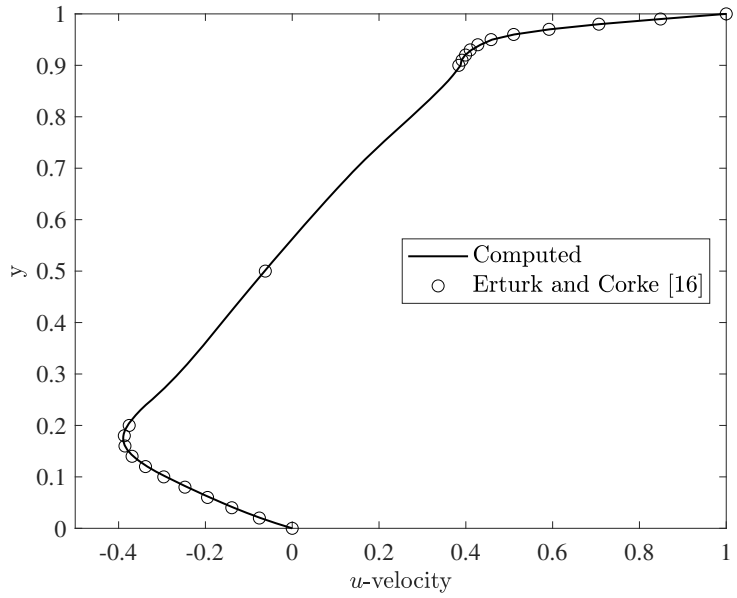

Figure 4: Computed u-velocity profile along a vertical line passing through the geometric centre of the cavity for the flow with $Re = 1000$.

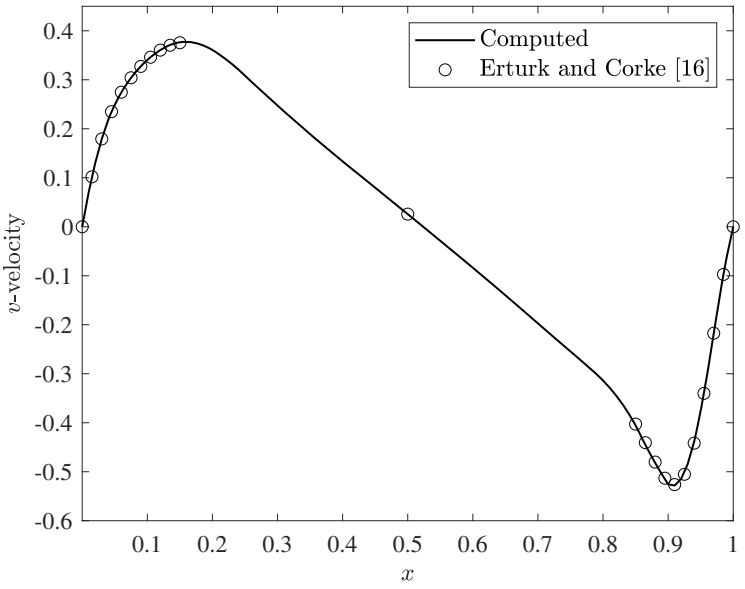

Figure 5: Computed v-velocity profile along a horizontal line passing through the geometric centre of the cavity for the flow with $Re = 1000$.

Vortex center locations

Table 2 presents the estimated coordinates of vortex centres for the flow with $Re = 1000$. The table compares the estimated coordinates with the four reference centre locations reported in [14, 15, 16, 17]. Also, the parameters, such as the grid mesh size and DOF from the corresponding studies, are shown in Table 2. The results obtained by the present method are in good agreement with the four reference centre locations. The best agreement of our results for $Re = 1000$ is with the results of Botella and Peyret [15], Erturk *et al*. [16], and Shapeev and Lin [17]. The relative errors in the centre location of PV, BR1, BL1 and BR2 between our work and [15, 16, 17] is less than 0.0024, and the relative error in the centre location of BL2 is less than 0.03.

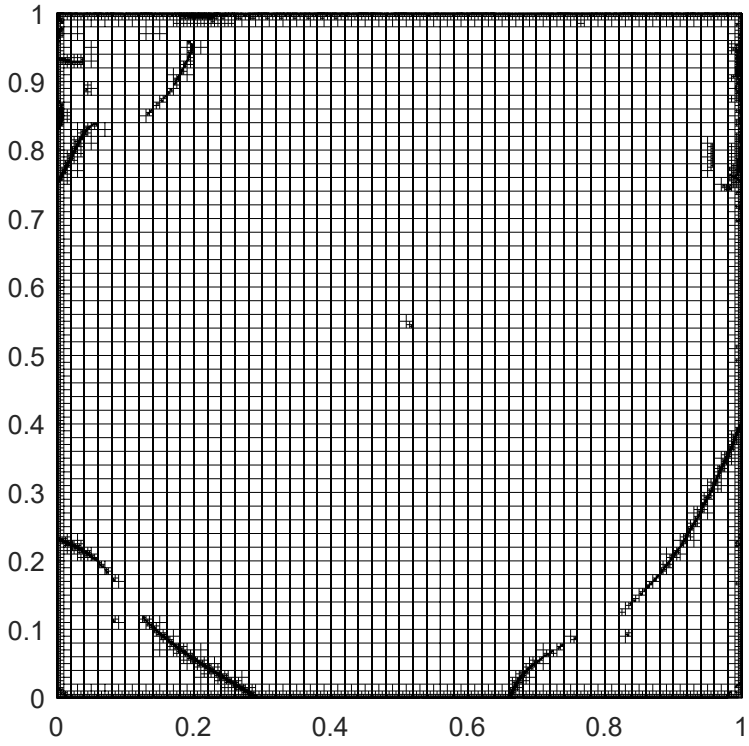

Figure 6: The tenth refined mesh, Mesh$_{10}$, for the flow with $Re = 2500$.

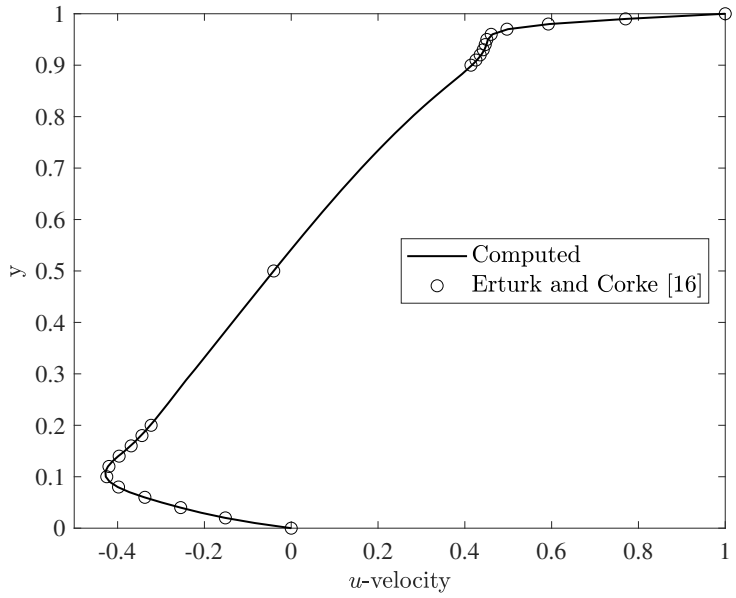

Figure 7: Computed u-velocity profile along a vertical line passing through the geometric centre of the cavity for the flow with $Re = 2500$.

Table 3 tabulates the estimated coordinates of vortex centres for the flow with $Re = 2500$. It compares it with the two reference centre locations reported in Erturk *et al.* [16], and Shapeev and Lin [17]. The centre locations obtained by the present method are in good agreement with that of Erturk *et al.* [16], and Shapeev and Lin [17]. The best agreement of our results for $Re = 2500$ is with the results of Shapeev and Lin [17], where the relative errors in the centre location of vortices between our work and [17] is less than 0.006. The relative errors in the centre location of PV, BR1, BL1, BR2 and TL1 between our work and Erturk *et al.* [16] is less

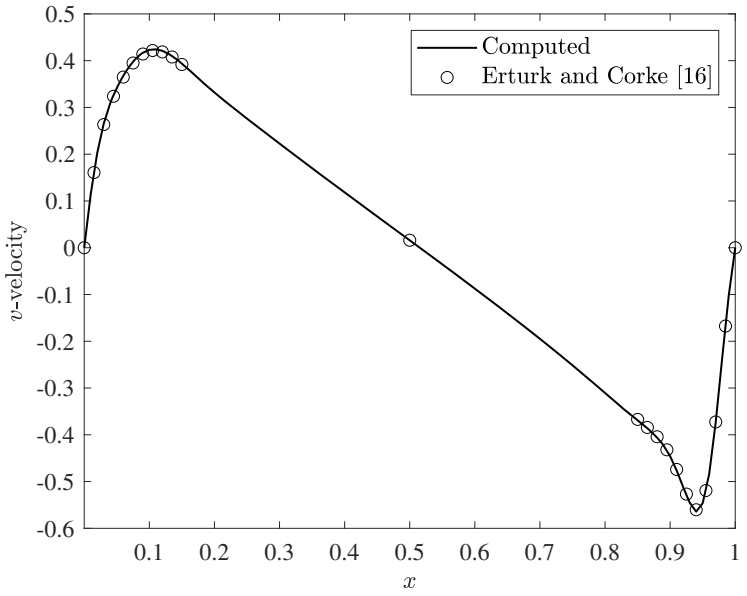

Figure 8: Computed v-velocity profile along a horizontal line passing through the geometric centre of the cavity for the flow with $Re = 2500$.

than 0.009, and the relative error in the centre location of BL2 is less than 0.08.

Figures 9 and 10 show streamlined contours and the flow features near the vortex centre for the flows with $Re = 1000$ and $Re = 2500$, respectively. The red dots in Figures 9 and 10 indicate the location of the centre of vortices (PV, BR1, BL1, BR2, BL2, and TL1) estimated using the AMR method.

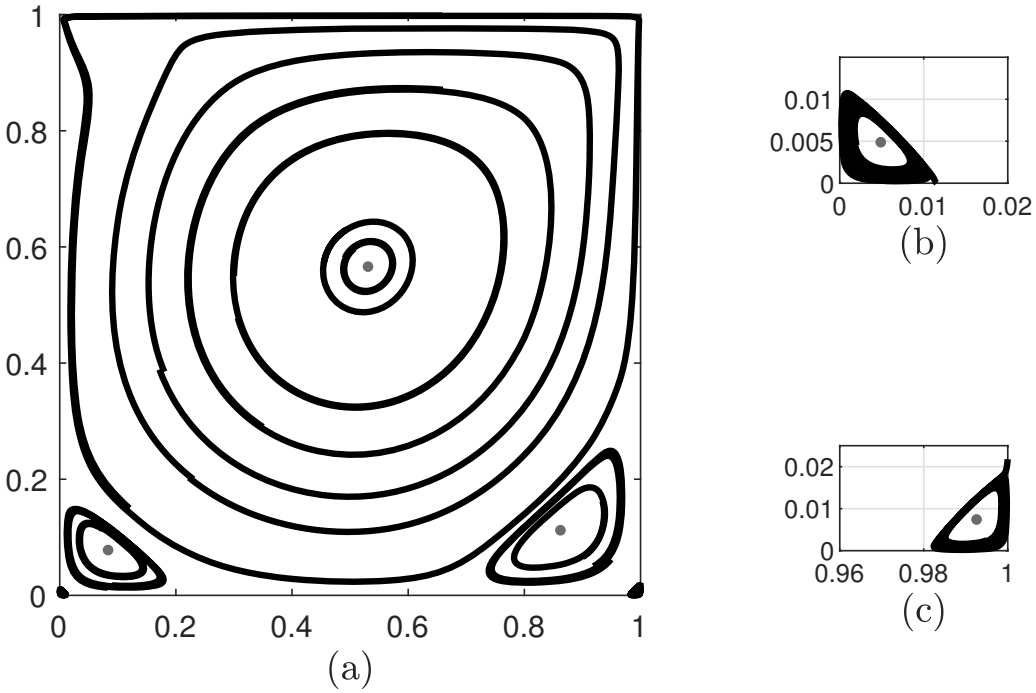

Figure 9: (a) $Re = 1000$: streamline contours and the location of centres of PV, BR1, BL1, BR2, and BL2. The zoomed-in sections of BR and BL show (b) BL2 and (c) BR2, respectively.

Table 2: Location of the centre of vortices for the flow with $Re = 1000$.

Vortex	Reference	Grid size, DOF	Centre location (x, y)
PV	Present	-, 615669	(0.530762, 0.566113)
	Ghia *et al.* [14]	129×129, 33282	(0.5313, 0.5625)
	Botella and Peyret [15]	160×160, 76164	(0.5308, 0.5652)
	Erturk *et al.* [16]	601×601, 722402	(0.5300, 0.5650)
	Shapeev and Lin [17]	-, 226574	(0.530790112, 0.565240557)
BR1	Present	-, 615669	(0.862109, 0.112109)
	Ghia *et al.* [14]	129×129, 33282	(0.8594, 0.1094)
	Botella and Peyret [15]	160×160, 76164	(0.8640, 0.1118)
	Erturk *et al.* [16]	601×601, 722402	(0.8633, 0.1117)
	Shapeev and Lin [17]	-, 226574	(0.86404006, 0.11180617)
BL1	Present	-, 615669	(0.0833008, 0.0780273)
	Ghia *et al.* [14]	129×129, 33282	(0.0859, 0.0781)
	Botella and Peyret [15]	160×160, 76164	(0.0833, 0.0781)
	Erturk *et al.* [16]	601×601, 722402	(0.0833, 0.0783)
	Shapeev and Lin [17]	-, 226574	(0.08327318, 0.078095725)
BR2	Present	-, 615669	(0.992578, 0.00742187)
	Ghia *et al.* [14]	129×129, 33282	(0.9922, 0.0078)
	Botella and Peyret [15]	160×160, 76164	(0.99232, 0.00765)
	Erturk *et al.* [16]	601×601, 722402	(0.9917, 0.0067)
	Shapeev and Lin [17]	-, 226574	(0.992324852, 0.007650979)
BL2	Present	-, 615669	(0.00488281, 0.00488281)
	Ghia *et al.* [14]	129×129, 33282	-
	Botella and Peyret [15]	160×160, 76164	(0.00490, 0.00482)
	Erturk *et al.* [16]	601×601, 722402	(0.0050, 0.0050)
	Shapeev and Lin [17]	-, 226574	(0.0048426963, 0.0048452406)

Conclusions

We further verified the accuracy of the 2D AMR method using two cases of 2D lid-driven cavity flow. A very coarse initial mesh was iteratively refined ten times, and a good estimate of the coordinates of the centre of vortices was obtained for flows considering $Re = 1000$ and $Re = 2500$. The accuracy of the estimates is further supported by the numerically computed u and v velocity profiles, which were in excellent agreement with the benchmark results. Further work will consider applying the 2D AMR method for flows with higher Reynolds numbers.

Table 3: Location of the centre of vortices for the flow with $Re = 2500$

.

Vortex	Reference	Grid size, DOF	Centre location (x, y)
	Present	-,1660092	(0.519629, 0.544043)
	Erturk *et al.* [16]	601×601, 722402	(0.5200, 0.5433)
PV	Shapeev and Lin [17]	-, 226574	(0.5197769, 0.5439244)
	Present	-, 1660092)	(0.833438, 0.090625)
	Erturk *et al.* [16]	601×601, 722402	(0.8333 , 0.0900)
BR1	Shapeev and Lin [17]	-, 226574	(0.8344014, 0.09075692)
	Present	-, 1660092	(0.0841992, 0.110918)
	Erturk *et al.* [16]	601×601, 722402	(0.0833, 0.1117)
BL1	Shapeev and Lin [17]	-, 226574	(0.08424181, 0.1110061)
	Present	-, 1660092	(0.990469, 0.00935125)
	Erturk *et al.* [16]	601×601, 722402	(0.9900, 0.0083)
BR2	Shapeev and Lin [17]	-, 226574	(0.9904594, 0.009384439)
	Present	-, 1660092	(0.00613281, 0.00621094)
	Erturk *et al.* [16]	601×601, 722402	(0.0067, 0.0067)
BL2	Shapeev and Lin [17]	-, 226574	(0.006129716, 0.006158831)
	Present	-, 1660092	(0.0434375, 0.889062)
	Erturk *et al.* [16]	601×601, 722402	(0.0433, 0.8900)
TL1	Shapeev and Lin [17]	-, 226574	(0.04300225, 0.8893601)

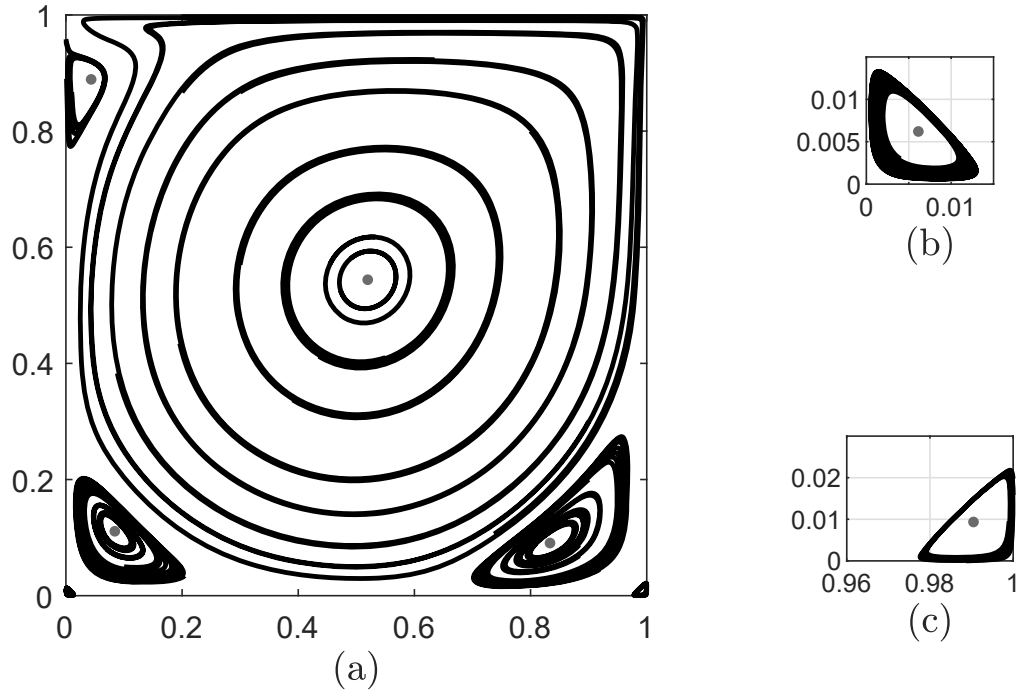

Figure 10: (a) $Re = 2500$: streamline contours and the location of centres of PV, BR1, BL1, BR2, BL2 and TL1. The zoomed-in sections of BR and BL show (b) BL2 and (c) BR2, respectively.

References

[1] Slotnick, J. P., Khodadoust, A., Alonso, J., Darmofal, D., Gropp, W., Lurie, E., and Mavriplis, D. J. (2013) CFD vision 2030 study: a path to revolutionary computational aerosciences. *NASA: Washington, DC, USA*

[2] Li, Z. (2017a) Computational complexity of the algorithm for a 2D adaptive mesh refinement method using lid-driven cavity flows. *Computational Thermal Sciences: An International Journal* **9**, 395–403.

[3] Plewa, T., Linde, T. J., and Weirs, V. G. (2005) Adaptive mesh refinement-theory and applications. In: Proceedings of the Chicago Workshop on Adaptive Mesh Refinement Methods. Springer-Verlag Berlin Heidelberg, 452–456

[4] Berger, M. and Oliger, J. (1984) Adaptive mesh refinement for hyperbolic partial differential equations. *Journal of Computational Physics* **53**, 484–512.

[5] Bell, J., Berger, M., Saltzman, J., and Welcome, M. (1994) Three-dimensional adaptive mesh refinement for hyperbolic conservation laws. *SIAM Journal on Scientific Computing* **15**, 127–138.

[6] Friedel, H., Grauer, R. and Marliani, C. (1997) Adaptive mesh refinement for singular current sheets in incompressible magnetohydrodynamic flows. *Journal of Computational Physics* **134**, 190–198.

[7] Berger, M. J, and Leveque, R. J. (1998) Adaptive mesh refinement using wave-propagation algorithms for hyperbolic systems. *SIAM Journal on Numerical Analysis* **35**, 2298–2316.

[8] Li, Z. (2008) An adaptive two-dimensional mesh refinement method based on the law of mass conservation. *Journal of Flow Visualization and Image Processing* **15**, 17–33.

[9] Li, Z. (2006) An adaptive streamline tracking method for three-dimensional CFD velocity fields based on the law of mass conservation. *Journal of Flow Visualization and Image Processing* **13**, 359–376.

[10] Lal, R. and Li, Z. (2015) Sensitivity analysis of a mesh refinement method using the numerical solutions of 2-D steady incompressible driven cavity flow. *Journal of Mathematical Chemistry* **53**, 844–867.

[11] Li, Z. (2017b) Analysis of 2D unsteady flow past a square cylinder at low Reynolds numbers with CFD and a mesh refinement method. *WSEAS Transactions on Fluid Mechanics* **12**, 150–157.

[12] Li, Z. and Li, M. (2021) Accuracy verification of a 2D adaptive mesh refinement method using backward-facing step flow of low Reynolds numbers. *International Journal of Computational Methods* **18**, 2041012.

[13] Li, Z., and Lal, R. (2023) Application of 2D adaptive mesh refinement method to estimation of the center of vortices for flow over a wall-mounted plate. *International Journal of Computational Methods* **20**, 2143012.

[14] Ghia, U. K. N. G., Ghia, K. N., and Shin, C. T. (1982) High-Re solutions for incompressible flow using the Navier-Stokes equations and a multigrid method. *Journal of Computational Physics* **48**, 387–411.

[15] Botella, O., & Peyret, R. (1998) Benchmark spectral results on the lid-driven cavity flow. *Computers and Fluids* **27**, 421–433.

[16] Erturk, E., Corke, T. C., & Gökçöl, C. (2005) Numerical solutions of 2-D steady incompressible driven cavity flow at high Reynolds numbers. *International Journal for Numerical Methods in fluids* **48**, 747–774.

[17] Shapeev, A. V., and Lin, P. (2009) An asymptotic fitting finite element method with exponential mesh refinement for accurate computation of corner eddies in viscous flows. *SIAM Journal on Scientific Computing* **31**, 1874–1900.